Nanoscale

Accepted Manuscript

This article can be cited before page numbers have been issued, to do this please use: A. Amorim Graf, M. Large, S. P. Ogilvie, Y. Rong, P. Lynch, G. Fratta, S. Ray, A. Shmeliov, V. Nicolosi, R. Arenal, A. A. King and A. B. Dalton, *Nanoscale*, 2019, DOI: 10.1039/C9NR04974F.

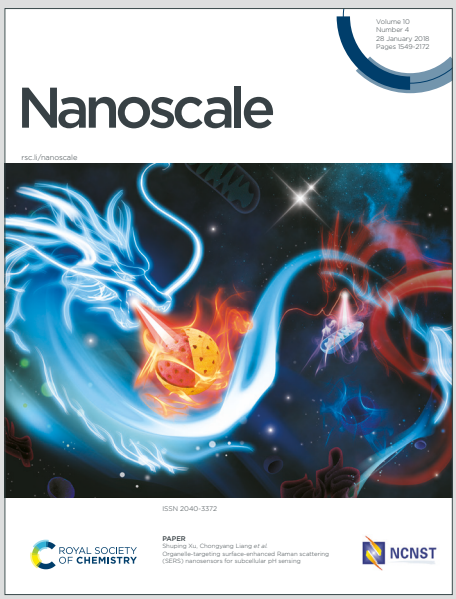

ROYAL SOCIETY OF CHEMISTRY

rsc.li/nanoscale

View Article Online
DOI: 10.1039/C9NR04974F

Sonochemical edge functionalisation of molybdenum disulfide

Aline Amorim Graf [†,*], Matthew J. Large[†], Sean P. Ogilvie[†], Yuanyang Rong[†], Peter J. Lynch[†], Giuseppe Fratta[†], Santanu Ray[‡], Aleksey Shmeliov[§], Valeria Nicolosi[§], Raul Arenal[□,ǁ,o], Alice A. K. King[†], and Alan B. Dalton[†,*]

[†] University of Sussex, Brighton, BN1 9QH, UK

[‡] Surface Analysis Laboratory, University of Brighton, Brighton, BN2 4GJ, UK

[§] Trinity College Dublin, School of Chemistry, CRANN, AMBER & I-Form, Dublin 2, Dublin, Ireland

[□] Laboratorio de Microscopias Avanzadas, Instituto de Nanociencia de Aragón, Universidad de Zaragoza, 50018 Zaragoza, Spain

[ǁ] ARAID Foundation, 50018 Zaragoza, Spain

[o] Instituto de Ciencias de Materiales de Aragon, CSIC-U. de Zaragoza, 50009 Zaragoza, Spain

ABSTRACT: Liquid-phase exfoliation (LPE) has been shown to be capable of producing large quantities of high-quality dispersions suitable for processing into subsequent applications. LPE typically requires surfactants for aqueous dispersions or organic solvents with high boiling point. However, they have major drawbacks such as toxicity, aggregation during solvent evaporation or the presence of residues. Here, dispersions of molybdenum disulfide in acetone are prepared and show much higher concentration and stability than predicted by Hansen parameter analysis. Aiming to understand those enhanced properties, the nanosheets were characterised using UV-visible spectroscopy, zeta potential measurements, atomic force microscopy, Raman spectroscopy, transmission electron microscopy, X-ray photoelectron spectroscopy and scanning transmission microscopy combined with spatially-resolved electron energy loss spectroscopy. Also, the performance of the MoS_2 nanosheets exfoliated in acetone was compared to those exfoliated in isopropanol as a catalyst for the hydrogen evolution reaction. The conclusion from the chemical characterisation was that MoS_2 nanosheets exfoliated in acetone have an oxygen edge-functionalisation, in the form of molybdenum

View Article Online
DOI: 10.1039/C9NR04974F

oxides, changing its interaction with solvents and explaining the observed high-quality and stability of the resulting dispersion in a low boiling point solvent. Exfoliation in acetone could potentially be applied as a pretreatment to modify the solubility of MoS_2 by edge-functionalisation.

INTRODUCTION

Layered materials are composed of two-dimensional (2D) sheets bonded strongly in-plane and stacked weakly through the van der Waals force. The enhanced mechanical[1,2], electrical[1,3], optical[3,4], and thermal[2] properties displayed by the two-dimensional materials have attracted the interest of scientists over the past 15 years[5]. Inorganic materials such as the transition metal dichalcogenides (TMDs) are of particular interest due to their broad range of semiconducting and optical properties.

Liquid-phase exfoliation (LPE) is a simple production technique that provides the highest yields of nanosheets in the shortest timeframes[6]. Solvent selection for LPE is typically performed using a model based on Hansen solubility parameters. Charles Hansen extended the Hildebrand solubility parameter formalism by hypothesising that the cohesive energy density can be resolved into contributions from three classes of intermolecular interactions.[7] This approach was first proposed to understand the solubility of polymers, for which it has proven very effective. However it can also be applied for dispersions of layered materials[8]. This formalism predicts high exfoliation yields and good dispersion stability if there is close matching of the solubility parameters of the solvent and the layered material.[9] As such, Hansen solubility parameter analysis makes it possible to develop liquid phase methods to disperse and process various layered materials in a general and reproducible way.

The most common organic solvents for liquid-phase exfoliation have a high boiling point, based on the correlation between surface tension and solubility parameters through the cohesive energy density. However, aggregation occurs during deposition of thin films due to the slow evaporation of high boiling point solvents[10]. Similarly, for fabrication of polymer composites, heat treatments above the boiling point of the solvent are usually required to remove them, which is impractical for very high boiling point solvents and incompatible with some polymers. Alternatively, surfactants in aqueous dispersions are used to

View Article Online
DOI: 10.1039/C9NR04974F

achieve high concentrations and stable dispersions[11,12]. While aqueous dispersions provide a lower boiling point alternative, it is difficult to remove any residual surfactant which may influence film or composite properties[13]. Other approaches such as washing with lower boiling point solvents are wasteful and may impact the properties of the produced structures[14]. A solvent exchange method has been used as a way of incorporating the advantages of low boiling point dispersions of layered materials with more effective exfoliating solvents[15]. While this provides a solution, it would be desirable to prepare dispersions in low boiling point solvents by direct exfoliation as a mean of reducing process complexity[13,16].

RESULTS AND DISCUSSION

Acetone is an example of a desirable low boiling point solvent for LPE as it is readily available, has low toxicity and is widely used. As such, dispersions of molybdenum disulfide (MoS_2) in acetone were prepared and found to have concentration and stability much higher than expected, according to the standard Hansen parameter model. Table 1 compares Hansen parameters of acetone and other conventionally used organic solvents[8] for LPE of MoS_2 (*N*-methyl-pyrrolidone and cyclopentanone), as well as Hansen interaction radius of those solvents with the nanomaterial. While the interaction radius for acetone is only ~50% greater than NMP and CPO, the attainable concentration exponentially decays with the square of the interaction radius[17]. Isopropanol (IPA) is another low boiling point solvent that has been used before to exfoliate layered materials, despite it being poorly Hansen matched[8,18,19], as seen in Table 1. There is also a high mismatch between the surface tension of acetone (23.4 mN/m) and the value for solvents which produced maximum concentration dispersions of layered materials (around 40 mN/m).[8]

View Article Online
DOI: 10.1039/C9NR04974F

Table 1. Hansen parameters for MoS_2[6,8] and different organic solvents: N-methyl-pyrrolidone (NMP), cyclopentanone (CPO), acetone and isopropanol (IPA).[7] The last column contains the respective calculated interaction radius to the layered material.

Material	Dispersive component ($MPa^{1/2}$)	Polar component ($MPa^{1/2}$)	Hydrogen bonding component ($MPa^{1/2}$)	Interaction radius to MoS_2 ($MPa^{1/2}$)
MoS_2	18.0	8.5	7.0	0
NMP	18.0	12.3	7.2	3.8
CPO	17.9	11.9	5.2	3.8
Acetone	15.5	10.4	7.0	5.4
IPA	15.8	6.1	16.4	10.7

Using metrics based on the extinction efficiency and confinement effects[20], it is possible to analyse the quality of the dispersion by estimating the concentration and the average layer number $\langle N \rangle$. Figure 1a shows a typical extinction spectrum with the position of both A and B exciton absorptions of MoS_2 indicated. An inset table contains values of both estimated dispersion properties over one year. Concentration was found to be higher than 0.1 mg/mL and the average layer number was estimated as approximately four. Both values are unexpected results for a low boiling point solvent with such a mismatch in the Hansen solubility parameters. Analysing the concentration and average layer number over a long time scale, it is inferred that the dispersion remains stable and the aggregation is minimal. Zeta potential measurements, shown in Figure 1b, corroborate the observed stability.[12,21,22] It is noted that the magnitude decreased by only 6% over more than a year.

View Article Online
DOI: 10.1039/C9NR04974F

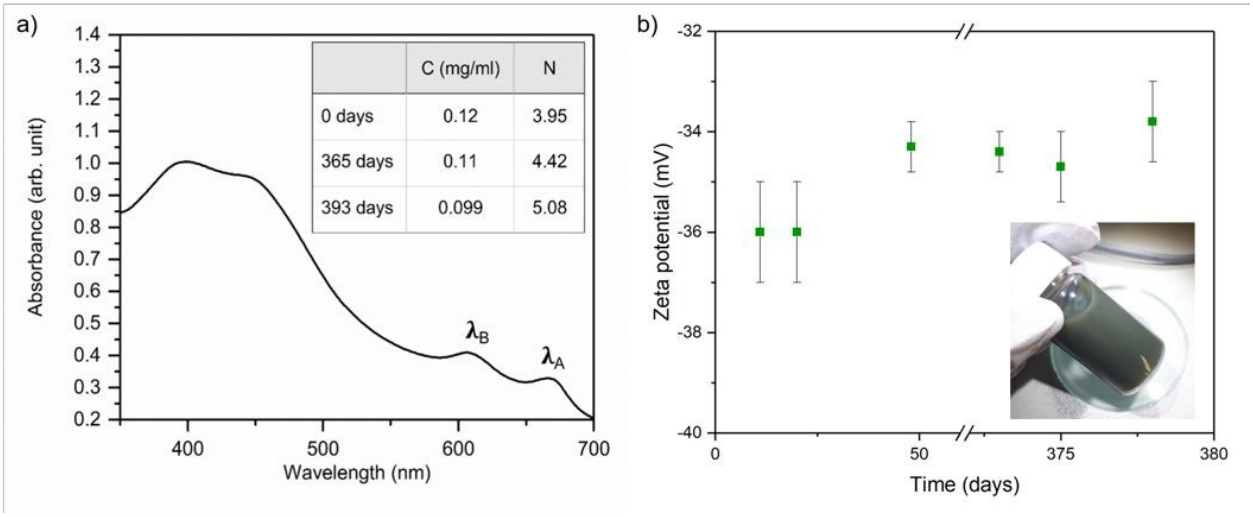

Figure 1. a) Representative extinction spectrum versus wavelength. The inset table contains the values for concentration (in mg/ml) and layer number over time. b) Zeta potential data shows that the dispersion is stable ($|\zeta| > 30\ mV$) for more than one year. A photograph of the high-quality dispersion is shown.

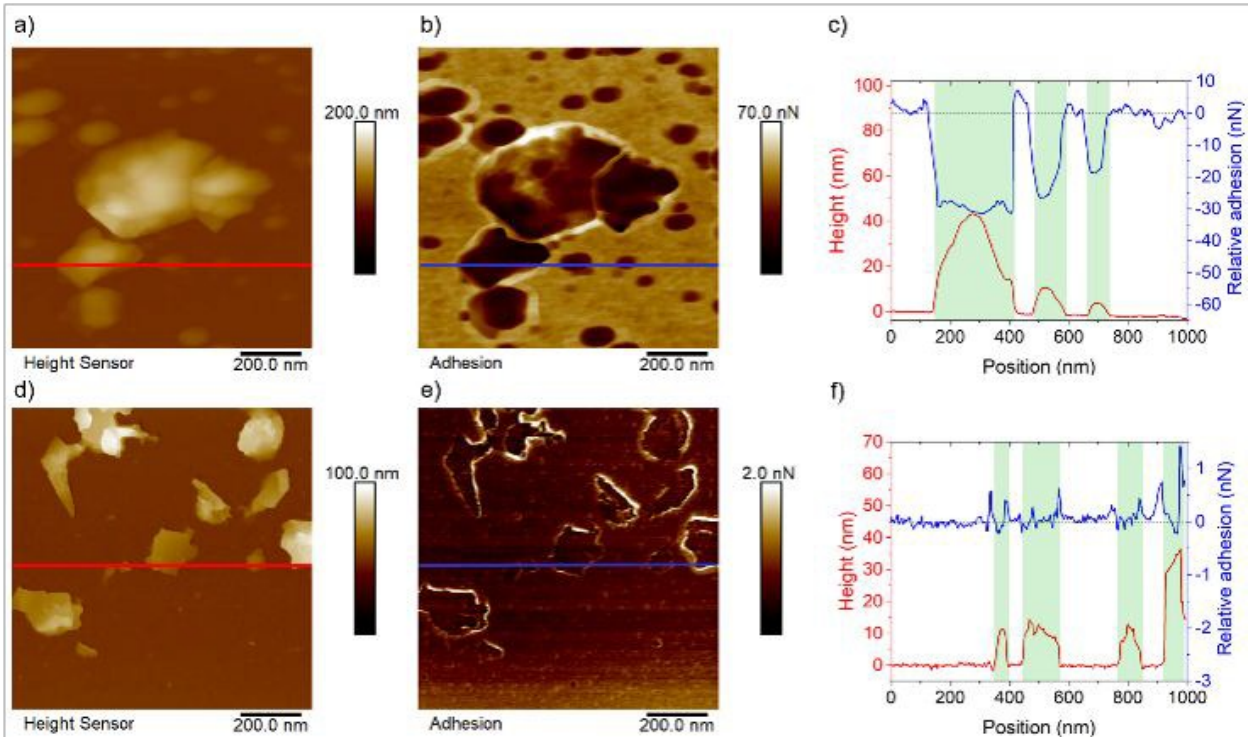

Figure 2. Atomic force microscopy (AFM) data for acetone-exfoliated (a, b and c) and IPA-exfoliated (d, e and f) nanosheets. a and d) Topography. b and e) Nanomechanical

View Article Online
DOI: 10.1039/C9NR04974F

adhesion. c and f) Graph comparing the topological and adhesion information for the line section marked. The nanosheets are highlighted.

In order to understand the enhanced properties of the acetone-exfoliated MoS_2, further characterisation was performed to identify any structural modification to the exfoliated nanosheets. Atomic force micrographs show that the nanosheets have a different morphology (Figure 2a) when comparing with MoS_2 exfoliated in isopropanol (IPA) using the same exfoliation parameters (Figure 2d). IPA is chosen as another low boiling point solvent and a molecular structural analogue for acetone. Line sections indicated on the micrographs of the height and adhesion channels (Figures 2a, 2b, 2d, 2e) are plotted separately in Figures 2c and 2f. The values for nanomechanical adhesion were offset to the average value for the substrate for both samples. There is a "halo", a region of higher adhesion surrounding the nanosheets exfoliated in acetone representing a higher interaction between the tip and nanosheets than tip and substrate. The feature is not observed in the height channel, as seen in Figure 2a. Also, the magnitude of adhesion forces is lower for the acetone-exfoliated nanosheets, which differs from the IPA sample, where adhesion for the flakes is the same as for the substrate. LPE has a broad size distribution, as seen in Figure 3 of the manuscript. This is particularly true since we have used a single centrifugation step for size selection. The relationship between physical thickness and layer number for LPE MoS_2 has been studied previously[20,23,24], with a monolayer thickness of 1.9 nm. In this case, thicknesses between approximately 2 nm and 20 nm correspond to 1-10 layer (i.e. 'few-layer') nanosheets, consistent with the average layer numbers measured and the Raman analysis presented. The UV-vis metrics employed are only calibrated to measure the average layer number. Additionally, the significant effect of the measurement parameters in the resulting thickness has been studied previously[25]. Equally, significantly larger particles (>>10 nm) are likely to be aggregates introduced during deposition of the dispersion for characterisation, due to the stochastic nature of the process.

View Article Online
DOI: 10.1039/C9NR04974F

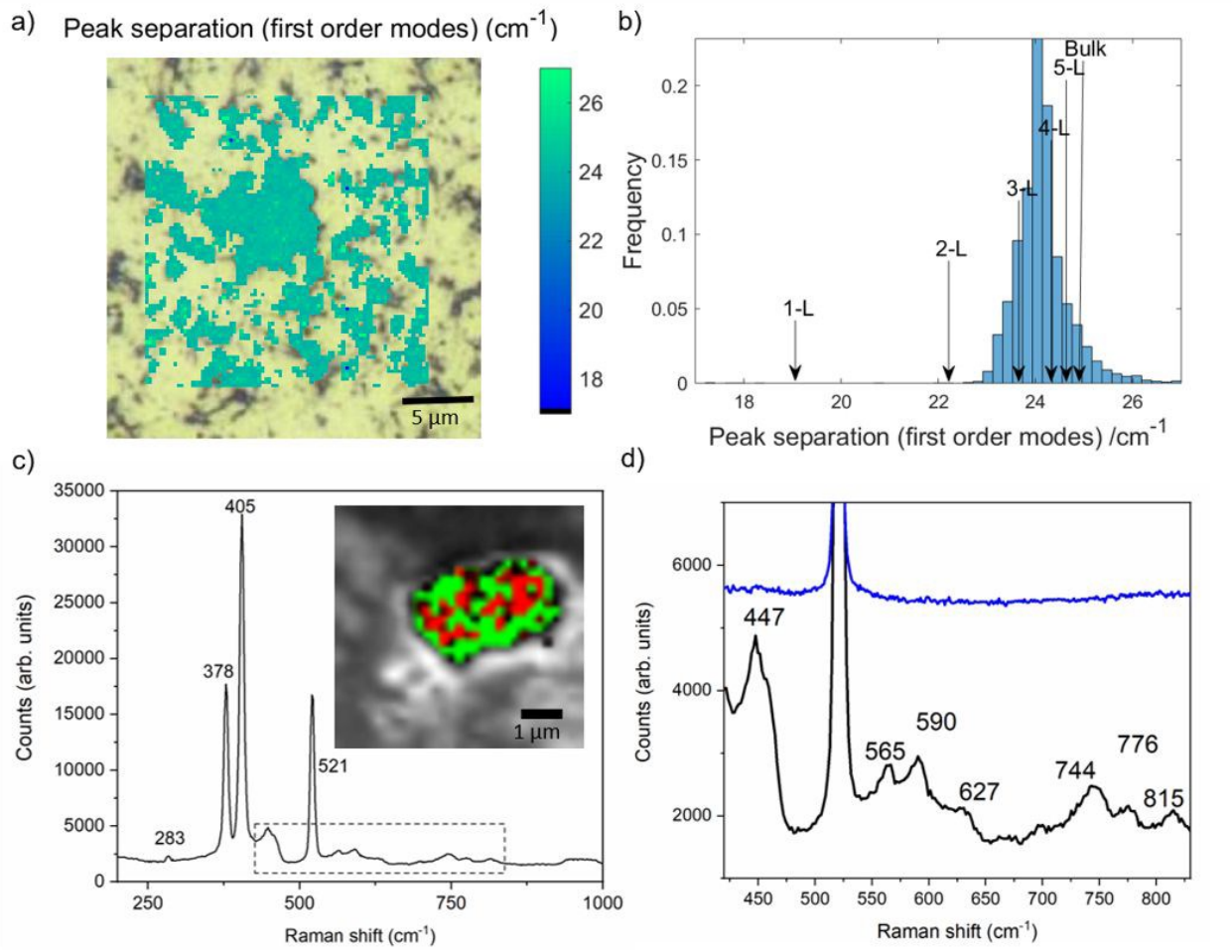

Figure 3. Raman spectra mapping. a) Peak separation map for resonant excitation. b) Histogram of the peak separation and the corresponding average layer number. c) Typical spectrum from the map is shown. Inset corresponds to mapping image. Colour scheme: green represents the MoS_2 peak; grey, silicon and red, molybdenum trioxide. d) Zoomed region from panel c showing additional peaks observed for acetone-exfoliated (black) in contrast with IPA-exfoliated nanosheets (blue).

Resonant Raman mapping was performed to statistically evaluate the degree of exfoliation over a large area. The separation of the two main MoS_2 peaks, the in-plane (E^1_{2g}) and the out-of-plane (A_{1g}) modes[26], for each pixel is plotted as a colour map (Figure 3a). The associated histogram of the peak separation, which is correlated with layer number distribution[27], is shown in Figure 3b. The histogram features a narrow asymmetric distribution with average peak separation of 24.2 cm^{-1} (standard deviation of 0.63 cm^{-1}).

View Article Online
DOI: 10.1039/C9NR04974F

Indicative values of the mode separation based on measurements of mechanically exfoliated MoS_2 from the literature suggest that the mean layer number in the sample is $\langle N \rangle \approx 4$, which is consistent with UV-vis measurements made previously. This supports the demonstration of high-quality exfoliation in a low-boiling point solvent.

Non-resonant Raman mapping (Figure 3c) shows the expected MoS_2 modes: the in-plane vibration (E^1_{2g}) at 378 cm^{-1} and the out-of-plane (A_{1g}) at 405 cm^{-1}. Acetone-exfoliated nanosheets shows a broader full width at half maximum for the out-of-plane mode when compared to the IPA-exfoliated material (see Figure S1 of Supporting Information). Literature about mechanically cleaved MoS_2[28] suggests the broadening may be associated with a higher defect density. The peak at 521 cm^{-1} is the silicon wafer substrate and the peak at 447 cm^{-1} is silicon oxide. The remaining modes are not present in dispersions of MoS_2 in IPA produced with the same exfoliation parameters (Figure 3d). Peaks at 590 and 776 cm^{-1} are vibrational modes of acetone. The samples have been treated above the boiling point of acetone before performing the characterisation to remove any residual solvent. The presence of those modes even after the heat treatment suggest a strong interaction between the nanosheets and acetone. The peaks at 283 and 815 cm^{-1} correspond to known modes of MoO_3, while the peak at 627cm^{-1} is associated with hydrates of MoO_3 [29,30]. The peaks at 565 and 744 cm^{-1} are associated with MoO_2 [31]. Mapping of the modes associated with the oxides and disulfide are shown in the inset of Figure 3c (in red and green, respectively). For the agglomerate mapped, the presence of the oxide peak is relatively uniform throughout the disulfide-containing areas, but the two are fundamentally co-localised. This suggests that particles of the oxides do not form in isolation from the disulfide nanosheets.

Following this indication of the presence of other molybdenum compounds in the samples, transmission electron microscopy was performed to evaluate the morphology of these additional components.

View Article Online
DOI: 10.1039/C9NR04974F

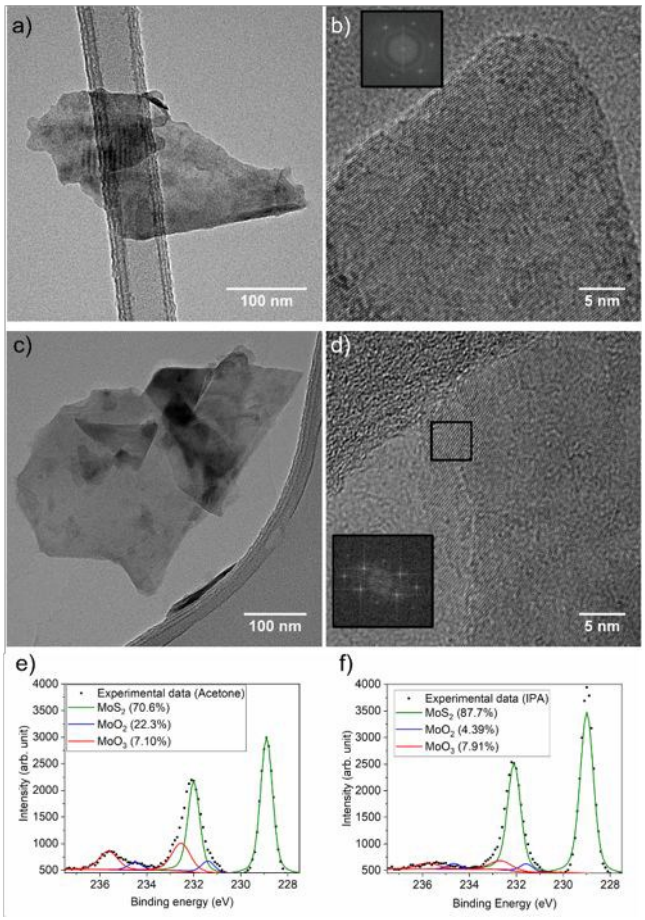

Figure 4. a) Representative TEM micrograph of MoS_2 exfoliated in isopropanol. b) Zoomed in TEM micrograph of the same dispersion with an inset showing the FFT as a regular hexagonal structure. c) Representative TEM micrograph of MoS_2 flake casted from the dispersion in acetone. d) Edge of an acetone-exfoliated MoS_2 flake. Inset shows a different pattern in the highlighted area corresponding to few-layered molydenum trioxide. e) XPS measurement showing binding energy in the range of molybdenum of acetone-exfoliated nanosheets show the expected MoS_2 structure with additional molybdenum oxide peaks. f) XPS data for IPA-exfoliated nanosheets in the same range.

Figure 4 shows transmission electron micrographs comparing MoS_2 flakes exfoliated in IPA (a and b) and acetone (c and d) using the same exfoliation process. Analysing various regions of multiple nanosheets (additional micrographs are shown in Figure S2 of Supporting Information) with fast Fourier transform (FFT) it is possible to identify different crystallographic structures. The usual hexagonal structure expected for this nanomaterial

View Article Online
DOI: 10.1039/C9NR04974F

is observed for the flakes exfoliated in both solvents, as seen in the inset of figure 4b. However, the edges of the acetone-exfoliated nanosheets have an orthorhombic pattern associated with few-layer molybdenum trioxide[32,33] (Figure 4d).

In order to confirm that the structural modification at the nanosheet edges corresponds to the chemical modification observed in the Raman spectroscopy, X-ray photoelectron spectroscopy (XPS) was employed to characterise the composition. The acetone-exfoliated sample was found to have 11.2 at.% molybdenum, 18.2 at.% sulfur and 16.0 at.% oxygen. This excess of molybdenum atoms in the sample when compared to sulfur atoms (see Figure S3 of Supporting Information for data) (the ratio is greater than 1:2) and the significant oxygen presence confirms the formation of other molybdenum-based compounds including MoO_2 and MoO_3, as shown in Figure 4e. The atomic percentages when analysing just the compounds containing molybdenum atoms are 70.6% for MoS_2, 22.3% for MoO_3 and 7.1% for MoO_2. For IPA-exfoliated nanosheets, the atomic percentages for molybdenum atoms are assigned to each compound as follows: 87.7% for MoS_2, 7.91% for MoO_3 and 4.39% for MoO_2. Even though some oxidation was observed for this sample, oxide content is significantly higher for acetone-exfoliated nanosheets.

View Article Online
DOI: 10.1039/C9NR04974F

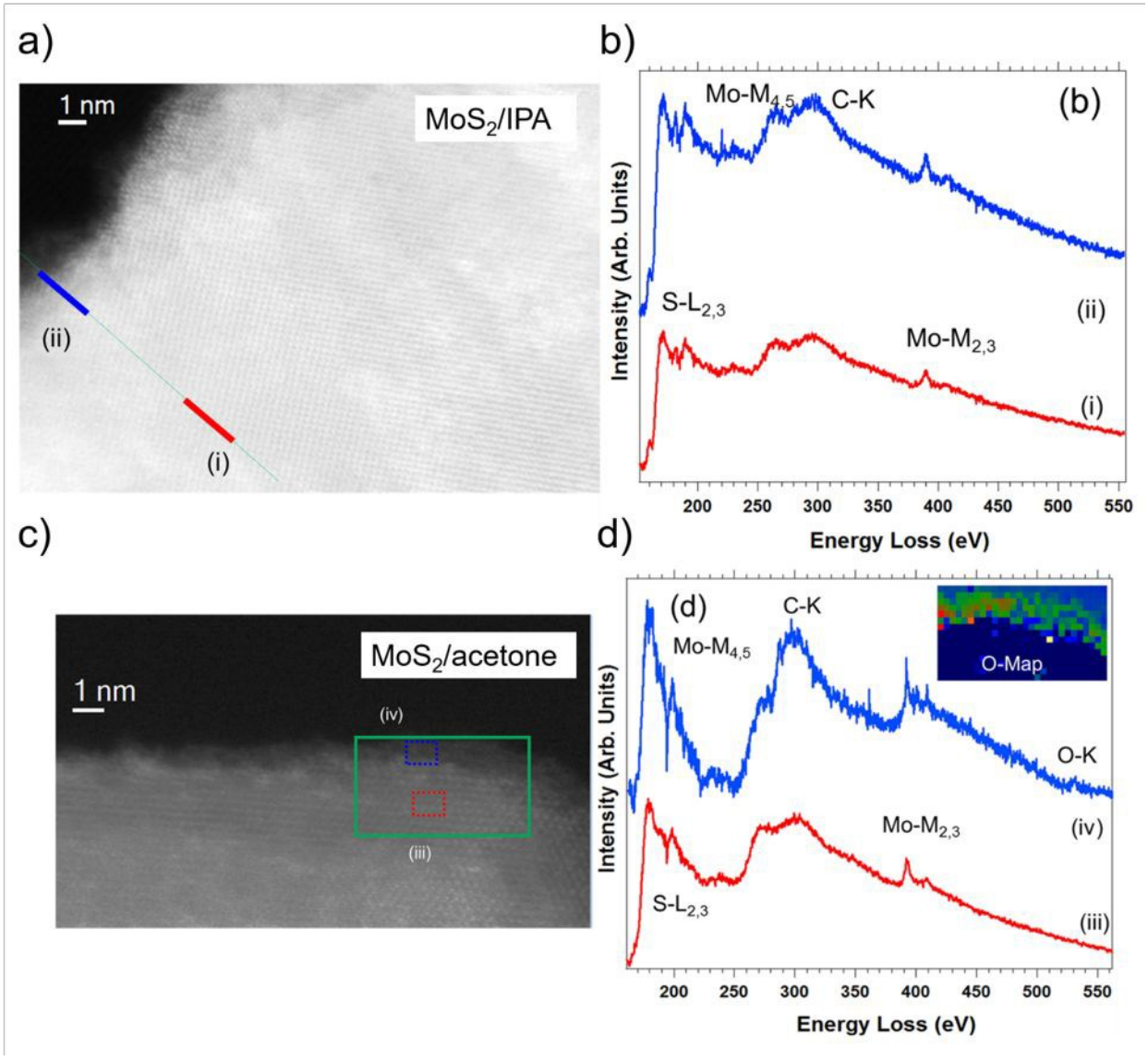

Figure 5: HAADF-STEM micrographs of two MoS_2 flakes from samples of two different MoS_2 dispersions: (a) IPA and (c) acetone. In the IPA-exfoliated MoS_2 nanosheet (a) an EELS spectrum-line was collected following the green marked line. (b) Two EELS spectra corresponding to the sum of 12 spectra collected in each of the two highlighted areas (red (i) and blue (ii)) of this spectrum-line of a). Sulfur and molybdenum (associated to the MoS_2) as well as some carbon are detected in these spectra. d) Two EEL spectra corresponding to the addition of 21 spectra recorded in each of the 2 regions highlighted in red (iii) and blue (iv) in the EELS spectrum-image obtained in the green marked area of c). The inset of this figure shows the O map obtained from this EELS spectrum-image.

View Article Online
DOI: 10.1039/C9NR04974F

Oxygen, which is likely associated to molybdenum oxide, is present at the edge of the flake, as clearly observed in this elemental map.

In order to get more detailed chemical and structural information of the effects of the dispersion of MoS_2 in different solvents at the local scale, aberration-corrected scanning transmission electron microscopy (STEM) was performed. High-angle annular dark field (HAADF) STEM combined with spatially-resolved electron energy loss spectroscopy (SR-EELS) is a powerful technique for getting this information[34,35]. Figures 5a and 5c show two HAADF-STEM images of two of these MoS_2 nanosheets exfoliated in IPA and acetone, respectively. Different EELS spectrum-lines (SPLI, 1D)/-images (SPIM, 2D) were recorded on these flakes. Figures 5a and 5c display the areas where an EELS SPLI and a SPIM have been collected (green highlighted areas). Two different EEL spectra, corresponding to the addition of 12 spectra in the regions marked in Figure 5a, are displayed in Figure 5b. The analysis of these EELS data indicates that the flakes from the IPA dispersion are composed of MoS_2 and that their composition is homogenous and uniform, even at the edges of the nanosheets. The C-K feature is visible in these spectra probably from a small carbon contamination. This situation is different in the case of the MoS_2 in acetone dispersion sample, as seen in Figure 5c and 5d. The edges present an amorphous layer of less than 1 nm. This layer contains some carbon and oxygen (see the O-map, inset of Figure 5d). The presence of this oxygen at the edge indicates the clear oxidation of this MoS_2 flake in this region agreeing with the other characterisation results performed on these samples.

As seen in literature[36–38], the chemical reaction for oxidation of MoS_2 in presence of oxygen gas is:

$$2MoS_2 + 7O_2 \rightarrow 2MoO_3 + 4SO_2$$

$$MoS_2 + 6MoO_3 \rightarrow 7MoO_2 + 2SO_2$$

$$2MoO_2 + O_2 \rightarrow 2MoO_3$$

Thermodynamically, the surface of MoS_2 tends to be oxidised when in contact with oxygen by oxygen adsorption or substitution. Density functional theory calculations show

View Article Online
DOI: 10.1039/C9NR04974F

that the kinetic energy barrier for oxidation is lowered when sulfur vacancies, which have a high prevalence at edge sites, are produced during exfoliation[39].

These equations suggest the formation of sulfur dioxide, which would outgas and prevent observation by the characterisation techniques employed here. However, a pungent, sulfur-like odour, different from acetone, was noticed in the as-produced samples. Sulfur dioxide gas is very soluble (reaching several hundred v/v) in several organic solvents, including acetone[40]. This adds some weight, albeit qualitative, to the series of reactions shown above. It suggests that the observed chemical modification to the nanosheets occurs through interaction with atmospheric oxygen rather than with the solvent as acetone has greater propensity to contain or produce dissolved oxygen or oxygen radicals during sonication.[41]

In order to study the timescales involved for the spontaneous functionalisation of MoS_2 during exfoliation in acetone, an experiment was performed where the sonication time during exfoliation was varied. Lateral size and concentration values were obtained from the metrics[20] using UV-vis spectra. Average nanosheets length decays exponentially while concentration increases until a saturation point is reached (Figure 6a). Zeta potential measurements (see Figure S4 of Supporting Information) show that the exfoliated nanosheets are stable in dispersion even after short sonication times. It is noted that the high stability and concentration originates from a self-limiting process since each measured property of the dispersions has the tendency to plateau after approximately 3 hours of sonication. The electronegativity of oxygen atoms is higher than sulfur, which will result in a stronger Mo-X bond polarisation with the delta-negative charge residing on the chalcogen atoms, producing a negative charge on the particle surface. As the proportion of MoO_n components in the nanosheets increases, one would expect an increase in the magnitude of the negative charge on the particles, as we observe. Also MoO_3 is shown to be readily exfoliable in solvents, which are too polar and/or low surface energy for exfoliation of MoS_2 (i.e. IPA cf. NMP)[32]. Importantly, adding MoO_3 edge functionality to MoS_2 nanosheets presents the possibility of tuning the solubility across this range of solvents, perhaps improving dispersibility in solvents such as acetone, which are otherwise poor for MoS_2.

View Article Online
DOI: 10.1039/C9NR04974F

Continuing quantifying how microscopic modification of the nanosheets by spontaneous edge-functionalisation influence macroscopic properties such as the interaction with the solvent, Hansen and Hildebrand solubility parameters were measured for both supernatant and sediment of the final centrifugation step after the sonication (see Supporting Information, Figures S5 and S6). Figure 6b shows the Hildebrand plot for a dispersion of MoS_2 nanosheets. NMP has the highest concentration which could be explained by its high susceptibility to ambient and sonochemical degradation.[42,43] The solvent degradation complicates the production of an identical reference sample to the solvent in dispersion for extinction spectroscopy, and may also interfere with the exfoliation and stabilisation processes[44]. Although it is known that good solvents for nanomaterials cannot solely be identified based on Hildebrand parameters[6], it is therefore interesting to note that this exfoliation in acetone produces materials whose solubility *is* well described by this model, which is inferred by comparing the width of the Gaussian fitting with literature values[6,8]. The observed modification in Hansen and Hildebrand solubility parameters reported is a direct result of the edge functionalisation of MoS_2 with MoO_3. The Hildebrand parameter for the nanosheets is 20.8±0.6 $MPa^{1/2}$. The accepted value of the solubility parameter for MoO_3 is 20.7 $MPa^{1/2}$ [32] and MoS_2 is 21.1 $MPa^{1/2}$ [6]. The oxidation processes shift the values of the parameters for the MoS_2 nanosheets closer to the value for acetone (19.9 $MPa^{1/2}$).This functionalisation is responsible for the improved dispersability in acetone and appears to make MoS_2 more selective to well Hildebrand matched solvents, as is the case for MoO_3[32].

Hansen parameters for 2-butanone[7], a linear ketone containing one extra carbon than acetone, are 16.0, 9.0 and 5.1 $MPa^{1/2}$, for dispersive, polar and hydrogen bonding components, respectively. Highly concentrated dispersions of TMDs in 2-butanone using bath sonication was obtained by Lobo et al.[45]. A similar degree of exfoliation was obtained by them, as indicated by peak separation of the in-plane and out-of-plane Raman modes for MoS_2 (24.2 cm^{-1} for acetone and 24.9 cm^{-1} for 2-butanone). However the sedimentation life-time is significantly lower for 2-butanone, despite it having a better Hansen matching (smaller interaction radius) and higher viscosity[46]. Chemical

View Article Online
DOI: 10.1039/C9NR04974F

characterisation (XPS) and microscopy (HRTEM and AFM micrographs) in that work[45] does not indicate the presence of molybdenum oxides. It is observed that the zeta potential for nanosheets exfoliated in acetone is significantly higher than for those reported in 2-butanone. It is inferred that this is due to edge functionalisation present in the acetone-exfoliated nanosheets, and that this is in turn responsible for the extended sedimentation time. Exfoliation in 2-butanone using the same parameters for acetone was performed and the nanosheets characterised using Raman spectroscopy (see Supporting Information Figure S7a). Oxides peaks were not observed for the sample, as clearly demonstrated by the second derivatives of the Raman spectra in Figure S7b. The high quality and stability observed in acetone-exfoliated MoS_2 nanosheets due to spontaneous edge-functionalisation seems to be unique to acetone because of a combination of factors such as dissolved oxygen content, low viscosity and low vapour pressure, independently of surface energy and Hansen parameters matching.

View Article Online
DOI: 10.1039/C9NR04974F

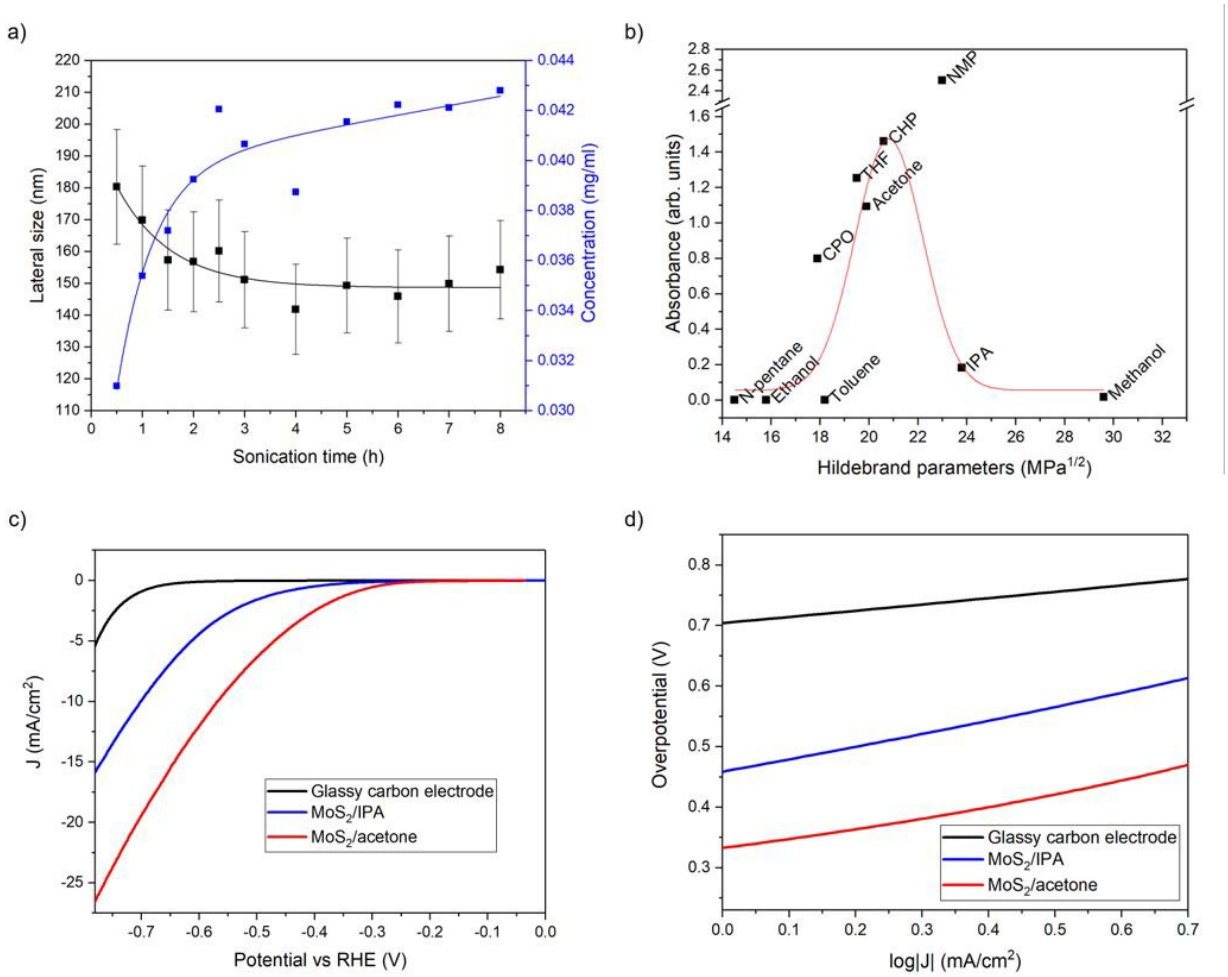

Figure 6. a) Length and concentration from metrics[20] plotted for different sonication times. b) Hildebrand solubility parameters for exfoliated MoS_2 nanosheets. c) Polarization curves for MoS_2 exfoliated in acetone (red) and IPA (blue). Reference substrate glassy carbon electrode is shown in black. d) Corresponding Tafel plots.

Exfoliated MoS_2 has been proposed as an efficient catalyst for the hydrogen evolution reaction (HER). Hydrogen is an environmentally-friendly alternative energy source to fossil fuel, and catalysts are necessary to increase the reaction efficiency to reach mass production levels. Platinum is known to be the best catalyst[47], however its high cost and unavailability in large quantities limit its use[48], and have prompted searches for alternative materials. Recent work has indicated that the edge sites and active site density on the edges of nanosheets are responsible for this catalytic activity[49,50] In order to investigate the effect of edge oxidation on the performance of MoS_2 nanosheets as HER catalysts,

View Article Online
DOI: 10.1039/C9NR04974F

MoS_2 exfoliated in acetone was compared against the same mass of MoS_2 prepared in IPA. The measurement was made by supporting the MoS_2 catalyst on a conductive and inert substrate (glassy carbon). Linear sweep voltammetry was used to measure the current against potential. For the HER, it is useful to offset the potential scale to the reversible hydrogen electrode (RHE), while the current is normalised to the electrode area,[51] as seen in Figure 6c. A superficial analysis of Figure 6c-d shows that the acetone-exfoliated nanosheets have a higher current density across the entire potential range which indicates its superiority.

Table 2. Hydrogen evolution characteristics of MoS_2 exfoliated in IPA and acetone.

	Tafel slope (mV/decade)	**Onset potential (V vs RHE)**	**J @ -0.4V (mA/cm^2)**	**Size (from UV-vis metrics)[20] (nm)**
MoS_2/IPA	193	-0.38	0.50	172
MoS_2/acetone	150	-0.27	2.51	212

Deeper analysis shows an onset potential, the potential value for which catalyst current is first observed, for hydrogen evolution at -0.27 V vs RHE and a current density of 2.51 mA/cm^2 at -0.4V for the sample prepared in acetone, shown in Table 2. The IPA sample shows a higher onset potential and a lower current density both of which result in an inferior hydrogen evolution catalyst. Figure 6d shows the Tafel curves of the J-V data displayed in Figure 6a. From the linear region of this curve we can extract the Tafel slope which is representative of the effectiveness of a material as a HER catalyst (lower is better) and the mechanism by which the H_3O^+ ions are reduced. The Tafel slope recorded is in the range attributed to MoS_2 in literature[47,48].

Of primary importance is that across all metrics, shown in Table 2, MoS_2 exfoliated in acetone exceeds the performance of that prepared in IPA in terms of hydrogen evolution efficiency. It is also interesting that the MoS_2 nanosheets exfoliated in acetone are significantly bigger than those prepared in IPA. The turnover frequency of MoS_2 hydrogen

View Article Online
DOI: 10.1039/C9NR04974F

evolution has been shown to be inversely proportional to the length and directly to the active site density[52]. This suggests that, while MoS_2 prepared in acetone is larger, it has much more active sites that participate in hydrogen evolution. This could be due to oxide groups having preferential energetics to hydrogen ion adsorption, electron transfer or lower steric hindrance. Also, the MoO_3 hydrophilic edges allow for better contact with electrolyte.[53]

CONCLUSIONS

The high concentration and stability of MoS_2 nanosheets dispersed in acetone is not fully explained by the Hansen solubility parameter model. Edge-functionalisation occurs spontaneously during ultrasonic exfoliation and produces molybdenum oxide, which fundamentally changes the main interaction of the nanosheets with the solvent. It is also observed that the edge functionalisation significantly modifies macroscopic properties resulting in an improved performance of acetone-exfoliated MoS_2 as a hydrogen evolution reaction catalyst, in comparison with material prepared in the same way using a structural analogue solvent (IPA). Evidence of functionalisation are observed with modification of solubility parameters and HER activity, which are known to be edge sensitive. Microscopic characterisation confirms the presence of oxygen-containing regions at the edges of the nanosheets. The exfoliation in acetone could be generally applied as a pretreatment to modify the solubility of layered materials by edge-functionalisation. In particular it is of interest to investigate whether the same chemistry is observed, under exfoliation conditions, for the other transition metal dichalcogenides, possibly bringing out useful properties.

EXPERIMENTAL PROCEDURE

Liquid-phase exfoliation of MoS_2. The dispersion of MoS_2 (Aldrich Chemistry) at initial concentration of 20 mg/mL (80 mL of total volume) was probe sonicated using the Sonics Vibracell VCX750 and the ½-inch (13 mm) tip for 1h at 60% amplitude. The resulting dispersion was centrifuged for 30 min at 5000g. The supernatant was discarded and the sediment was redispersed into 80 mL of acetone (VWR Chemicals) or IPA (Fisher Chemical), as received. The dispersion was probe sonicated for 5h at 60% amplitude,

View Article Online
DOI: 10.1039/C9NR04974F

pulsed 6s on and 2s off. It was then centrifuged for 5 min at 5000g. The supernatant was collected for further characterisation.

UV-vis spectroscopy. UV-vis spectra were measured in quartz cuvettes using the Shimadzu UV-3600 Plus spectrophotometer.

Zeta potential. Zeta potential was measured in the AntonPaar Litesizer 500 particle analyser. The sample was prepared diluting 10 µL of MoS_2/acetone dispersion in 350 ml of deionized water. A Thermo Scientific Barnstead MicroPure purification system was used to prepare ultrapure water (18.2 MΩ resistivity). A potential difference of 200 mV was applied to an Omega cuvette containing the sample.

Sonication time study. For this study, a dispersion was prepared at the same initial concentration of 20 mg/mL but with total volume of 50 mL. It was probe sonicated using a Sonics Vibracell VCX130 with ¼-inch (6.3 mm) tip for 1h at 60% amplitude and centrifuged for 30 min at 5000g. The supernatant was discarded and the sediment redispersed into 50 mL of acetone. The dispersion was sonicated at 60% amplitude for times ranging between 30 min and 8h. Samples of 5 mL were collected every 30 min up until 3h and then every hour. Fresh solvent was added to keep the total volume constant during sonication. Every sample was centrifuged for 5 min at 5000g and the resulting supernatant was further characterised.

Hansen and Hildebrand parameters. A MoS_2 dispersion in acetone was prepared as described above. In order to measure the Hansen and Hildebrand solubility parameters for the material a total of 10 samples were prepared by centrifuging 2 mL of the supernatant of the final centrifugation step using Beckman Coulter's Optima TLX ultracentrifuge at 70,000 rpm (265,070g) for 20 minutes. Additional 10 samples were prepared by redispersing the sediment from the initial centrifugation step during preparation in fresh acetone and centrifuging them in the ultracentrifuge for 5 minutes at 5,000 rpm (1,350g). For both sets of centrifuge tubes the supernatant was discarded and 2 mL of solvent was added to each tube: N-pentane, ethanol, toluene, tetrahydrofuran, acetone, N-methyl-2-pyrrolidone, methanol (VWR Chemicals), cyclopentanone, 1-cyclohexyl-2-pyrrolidone (Aldrich Chemistry) and isopropanol (Fisher Chemical). Each

View Article Online
DOI: 10.1039/C9NR04974F

sample was sonicated for 10 seconds at 30% amplitude using Sonics Vibracell VCX130 with ¼-inch (6.3 mm) tip to redisperse the sediment into each solvent. These samples represent identical dispersions of particles (either exfoliated MoS_2 or bulk MoS_2) in different solvents of known solubility parameters. The stable concentrations achieved after a period of sedimentation allow the corresponding parameters of the particulates to be estimated. Samples were characterised using UV-vis spectroscopy.

Atomic force microscopy. The characterisation technique was employed with the Dimension Icon system from Bruker operating in the Peak Force Tapping mode (Quantitative Nanomechanical property mapping). This mode allows for topographic as well as nanomechanical properties characterisation. The probe used was a ScanAsyst Air tip whose spring constant is 0.4 N/m. The sample was prepared drop casting the MoS_2/acetone dispersion on silicon wafer. The wafer was heated above the boiling point of acetone (60°C) to remove any residual solvent in the analysed sample.

Raman spectroscopy. A Raman spectra map was measured on the same sample used for AFM characterisation. The non-resonant map was taken with an excitation laser wavelength of 532 nm and a 2400 l/mm grating. For the resonant map a 660nm laser was used with an 1800/mm grating. For both maps, step size was 0.25 μm in a square area of 20 μm side, 1s as integration time per point, power of 5 mV and optical magnification of 100x.

Transmission Electron Microscopy. Micrographs were taken using FEI Titan 80 – 300 scanning transmission electron microscope (STEM) operating at 300kV. The samples were deposited onto ultrathin carbon grid (standard lacey with 2 nm film on the top). Fast Fourier transform pattern was created using the ImageJ software.

X-ray photoelectron spectroscopy. Analysis was carried out using an ESCALAB 250 Xi system (Thermo Scientific) equipped with a monochromated Al K_α X-ray source. Uniform charge neutralization was provided by multi-mode electrostatic flood source. The standard analysis spot of ca. 900x900 μm^2 was defined by the microfocused X-ray source. Full survey scans (step size 1 eV, pass energy 150 eV, dwell time 50 ms and 5 scans) and narrow scans (step size 0.1 eV, pass energy 20 eV, dwell time 100 ms and

View Article Online
DOI: 10.1039/C9NR04974F

15 scans) of the Mo3d (binding energy, BE~229 eV), S2p (binding energy, BE ~162 eV), C1s (BE ~285 eV) and O1s (BE~531 eV) were acquired from four separate regions on each sample. Data were analysed using Thermo Avantage Software (Version 5.952) using a smart background.

Electron energy loss spectroscopy. The scanning transmission electron microscopy (STEM) imaging studies were performed on probe-corrected FEI Titan Low-Base 60-300 microscope operating at 200 kV (fitted with a X-FEG® gun, a Cs-probe corrector (CESCOR from CEOS GmbH)). EEL spectra were recorded using the spectrum-imaging (SPIM in 2D or spectrum-line (SPLI) in 1D) mode in a Gatan GIF Tridiem ESR 865 spectrometer. The convergent semi-angle was of 25 mrad, the collection semi-angle was of 80 mrad and the energy resolution ~ 1.0 eV. The EEL spectra were denoised with the open-source program Hyperspy by using principal component analysis routines.

Electrochemical characterisation. Measurements were performed in a three-electrode configuration with a Gamry potentiostat. Glassy carbon electrodes were used as the working electrode (3 mm diameter, BASi), while platinum wire and Ag/AgCl (3M KCl) were used as the counter and the reference electrode, respectively. A total mass of 13.4 µg of MoS_2 exfoliated in acetone was deposited onto the glassy carbon electrode with a catalyst loading of 0.2 mg/cm^2. In comparison, the same mass of MoS_2 exfoliated in IPA was deposited in the same way. Linear sweep voltammetry (LSV) experiments were performed with a scan rate of 5 mV/s from 0 V to -1 V (vs RHE) in 0.5M H_2SO_4 to investigate the hydrogen evolution performance. The measured potential was converted to the RHE scale by adding +0.210 V, measured with respect to a Gaskatel Hydroflex H_2 reference electrode.

ASSOCIATED CONTENT

Supplementary Information.

FWHM histogram of Raman mode

Additional TEM micrographs

XPS data for acetone-exfoliated nanosheets in the range of sulfur energy

View Article Online
DOI: 10.1039/C9NR04974F

Zeta potential characterisation for sonication time study

Hansen and Hildebrand solubility parameters results

Raman map for MoS_2 nanosheets exfoliated in 2-butanone

AUTHOR INFORMATION

Corresponding authors

Aline Amorim Graf (a.amorim-graf@sussex.ac.uk) or Alan B. Dalton (a.b.dalton@sussex.ac.uk)

Conflicts of Interest

There are no conflicts to declare.

Author contributions

ABD, AAG, MJL developed the study concepts. AAG, SPO, GF performed experiments. YR, PJL performed electrochemical characterisation. SR performed XPS. AS, VN performed TEM characterisation. RA performed SR-EELS. AAG, MJL, SPO prepared the manuscript. MJL, SPO, AAKK, ABD reviewed the final manuscript. All authors discussed the results and commented on the manuscript.

ACKNOWLEDGMENTS

The SR-EELS studies were conducted at the Laboratorio de Microscopias Avanzadas (LMA) at the Instituto de Nanociencia de Aragon (INA) - Universidad de Zaragoza (Spain). This project has received funding from the European Union's Horizon 2020 research and innovation programme under the Marie Sklodowska-Curie grant agreement No 642742 and under the "Graphene Flagship" project grant agreement No 785219. R.A. also acknowledges the support from the Spanish Ministerio de Economia y Competitividad (MAT2016-79776-P), from the Government of Aragon and the European Social Fund under the project "Construyendo Europa desde Aragon" 2014-2020 (grant number E13_17R). VN wishes to thank the support of SFI (AMBER and I-Form centres, PIYRA and US-Ireland grants) and the ERC CoG (3D2DPrint).

REFERENCES

1 A. K. Geim, *Science*, 2009, **324**, 1530–1534.
2 Q. Cai, D. Scullion, A. Falin, K. Watanabe, T. Taniguchi, Y. Chen, E. J. G. Santos and L. H. Li, *Nanoscale*, 2017, **9**, 3059–3067.
3 Q. H. Wang, K. Kalantar-Zadeh, A. Kis, J. N. Coleman and M. S. Strano, *Nat. Nanotechnol.*, 2012, **7**, 699–712.
4 A. Splendiani, L. Sun, Y. Zhang, T. Li, J. Kim, C.-Y. Chim, G. Galli and F. Wang, *Nano Lett.*, 2010, **10**, 1271–1275.

View Article Online
DOI: 10.1039/C9NR04974F

5 V. Nicolosi, M. Chhowalla, M. G. Kanatzidis, M. S. Strano and J. N. Coleman, *Science*, 2013, **340**, 1226419–1226419.
6 G. Cunningham, M. Lotya, C. S. Cucinotta, S. Sanvito, S. D. Bergin, R. Menzel, M. S. P. Shaffer and J. N. Coleman, *ACS Nano*, 2012, **6**, 3468–3480.
7 C. M. Hansen, *Hansen solubility parameters: a user's handbook*, CRC Press, Boca Raton, 2nd ed., 2007.
8 J. N. Coleman, M. Lotya, A. O'Neill, S. D. Bergin, P. J. King, U. Khan, K. Young, A. Gaucher, S. De, R. J. Smith, I. V. Shvets, S. K. Arora, G. Stanton, H.-Y. Kim, K. Lee, G. T. Kim, G. S. Duesberg, T. Hallam, J. J. Boland, J. J. Wang, J. F. Donegan, J. C. Grunlan, G. Moriarty, A. Shmeliov, R. J. Nicholls, J. M. Perkins, E. M. Grieveson, K. Theuwissen, D. W. McComb, P. D. Nellist and V. Nicolosi, *Science*, 2011, **331**, 568–571.
9 M. J. Large, S. P. Ogilvie, A. A. K. King and A. B. Dalton, *Langmuir*, 2017, **33**, 14766–14771.
10 K.-G. Zhou, N.-N. Mao, H.-X. Wang, Y. Peng and H.-L. Zhang, *Angew. Chem. Int. Ed.*, 2011, **50**, 10839–10842.
11 A. O'Neill, U. Khan and J. N. Coleman, *Chem. Mater.*, 2012, **24**, 2414–2421.
12 M. Lotya, Y. Hernandez, P. J. King, R. J. Smith, V. Nicolosi, L. S. Karlsson, F. M. Blighe, S. De, Z. Wang, I. T. McGovern, G. S. Duesberg and J. N. Coleman, *J. Am. Chem. Soc.*, 2009, **131**, 3611–3620.
13 A. O'Neill, U. Khan, P. N. Nirmalraj, J. Boland and J. N. Coleman, *J. Phys. Chem. C*, 2011, **115**, 5422–5428.
14 L. Xu, J.-W. McGraw, F. Gao, M. Grundy, Z. Ye, Z. Gu and J. L. Shepherd, *J. Phys. Chem. C*, 2013, **117**, 10730–10742.
15 X. Zhang, A. C. Coleman, N. Katsonis, W. R. Browne, B. J. van Wees and B. L. Feringa, *Chem. Commun.*, 2010, **46**, 7539.
16 V. Forsberg, R. Zhang, J. Bäckström, C. Dahlström, B. Andres, M. Norgren, M. Andersson, M. Hummelgård and H. Olin, *PLOS ONE*, 2016, **11**, e0154522.
17 J. N. Coleman, *Acc. Chem. Res.*, 2013, **46**, 14–22.
18 H. Liu, L. Xu, W. Liu, B. Zhou, Y. Zhu, L. Zhu and X. Jiang, *J. Colloid Interface Sci.*, 2018, **515**, 27–31.
19 J. Shen, Y. He, J. Wu, C. Gao, K. Keyshar, X. Zhang, Y. Yang, M. Ye, R. Vajtai, J. Lou and P. M. Ajayan, *Nano Lett.*, 2015, **15**, 5449–5454.
20 C. Backes, R. J. Smith, N. McEvoy, N. C. Berner, D. McCloskey, H. C. Nerl, A. O'Neill, P. J. King, T. Higgins, D. Hanlon, N. Scheuschner, J. Maultzsch, L. Houben, G. S. Duesberg, J. F. Donegan, V. Nicolosi and J. N. Coleman, *Nat. Commun.*, 2014, **5**, 4576.
21 A. Gupta and S. Vasudevan, *J. Phys. Chem. C*, 2018, **122**, 19243–19250.
22 R. J. Smith, M. Lotya and J. N. Coleman, *New J. Phys.*, 2010, **12**, 125008.
23 C. Backes, K. R. Paton, D. Hanlon, S. Yuan, M. I. Katsnelson, J. Houston, R. J. Smith, D. McCloskey, J. F. Donegan and J. N. Coleman, *Nanoscale*, 2016, **8**, 4311–4323.
24 K. R. Paton, E. Varrla, C. Backes, R. J. Smith, U. Khan, A. O'Neill, C. Boland, M. Lotya, O. M. Istrate, P. King, T. Higgins, S. Barwich, P. May, P. Puczkarski, I. Ahmed, M. Moebius, H. Pettersson, E. Long, J. Coelho, S. E. O'Brien, E. K. McGuire, B. M.

View Article Online
DOI: 10.1039/C9NR04974F

Sanchez, G. S. Duesberg, N. McEvoy, T. J. Pennycook, C. Downing, A. Crossley, V. Nicolosi and J. N. Coleman, *Nat. Mater.*, 2014, **13**, 624–630.
25 P. Nemes-Incze, Z. Osváth, K. Kamarás and L. P. Biró, *Carbon*, 2008, **46**, 1435–1442.
26 H. Li, Q. Zhang, C. C. R. Yap, B. K. Tay, T. H. T. Edwin, A. Olivier and D. Baillargeat, *Adv. Funct. Mater.*, 2012, **22**, 1385–1390.
27 J.-U. Lee, J. Park, Y.-W. Son and H. Cheong, *Nanoscale*, 2015, **7**, 3229–3236.
28 S. Mignuzzi, A. J. Pollard, N. Bonini, B. Brennan, I. S. Gilmore, M. A. Pimenta, D. Richards and D. Roy, *Phys. Rev. B*, 2015, **91**, 1954111–7.
29 B. C. Windom, W. G. Sawyer and D. W. Hahn, *Tribol. Lett.*, 2011, **42**, 301–310.
30 L. Seguin, M. Figlarz, R. Cavagnat and J.-C. Lassègues, *Spectrochim. Acta. A. Mol. Biomol. Spectrosc.*, 1995, **51**, 1323–1344.
31 M. Dieterle and G. Mestl, *Phys. Chem. Chem. Phys.*, 2002, **4**, 822–826.
32 D. Hanlon, C. Backes, T. M. Higgins, M. Hughes, A. O'Neill, P. King, N. McEvoy, G. S. Duesberg, B. Mendoza Sanchez, H. Pettersson, V. Nicolosi and J. N. Coleman, *Chem. Mater.*, 2014, **26**, 1751–1763.
33 A. Chithambararaj, N. Rajeswari Yogamalar and A. C. Bose, *Cryst. Growth Des.*, 2016, **16**, 1984–1995.
34 R. Arenal, K. March, C. P. Ewels, X. Rocquefelte, M. Kociak, A. Loiseau and O. Stéphan, *Nano Lett.*, 2014, **14**, 5509–5516.
35 F. L. Deepak, A. Mayoral and R. Arenal, Eds., *Advanced Transmission Electron Microscopy*, Springer International Publishing, Cham, 2015.
36 P. Kumar, M. Singh and G. B. Reddy, *Mater. Res. Express*, 2017, **4**, 036405.
37 P. Budania, P. Baine, J. Montgomery, C. McGeough, T. Cafolla, M. Modreanu, D. McNeill, N. Mitchell, G. Hughes and P. Hurley, *MRS Commun.*, 2017, **7**, 813–818.
38 Y. Shigegaki, S. K. Basu, M. Wakihara and M. Taniguchi, *J. Therm. Anal.*, 1988, **34**, 1427–1440.
39 S. Kc, R. C. Longo, R. M. Wallace and K. Cho, *J. Appl. Phys.*, 2015, **117**, 135301.
40 D. Flaxbart, *J. Am. Chem. Soc.*, 1999, **121**, 2339–2339.
41 C. Franco and J. Olmsted III, *Talanta*, 1990, **37**, 905–909.
42 H. C. Yau, M. K. Bayazit, J. H. G. Steinke and M. S. P. Shaffer, *Chem. Commun.*, 2015, **51**, 16621–16624.
43 A. Jawaid, D. Nepal, K. Park, M. Jespersen, A. Qualley, P. Mirau, L. F. Drummy and R. A. Vaia, *Chem. Mater.*, 2016, **28**, 337–348.
44 S. P. Ogilvie, M. J. Large, G. Fratta, M. Meloni, R. Canton-Vitoria, N. Tagmatarchis, F. Massuyeau, C. P. Ewels, A. A. K. King and A. B. Dalton, *Sci. Rep.*, 2017, **7**, 16706.
45 K. Lobo, S. Trivedi and H. S. S. R. Matte, *Nanoscale*, 2019, **11**, 10746–10755.
46 J. A. Dean and N. A. Lange, Eds., *Lange's handbook of chemistry*, McGraw-Hill, New York, NY, 15. ed., 1999.
47 D. McAteer, Z. Gholamvand, N. McEvoy, A. Harvey, E. O'Malley, G. S. Duesberg and J. N. Coleman, *ACS Nano*, 2016, **10**, 672–683.
48 Y. Yu, S.-Y. Huang, Y. Li, S. N. Steinmann, W. Yang and L. Cao, *Nano Lett.*, 2014, **14**, 553–558.
49 T. F. Jaramillo, K. P. Jorgensen, J. Bonde, J. H. Nielsen, S. Horch and I. Chorkendorff, *Science*, 2007, **317**, 100–102.

View Article Online
DOI: 10.1039/C9NR04974F

50 B. Hinnemann, P. G. Moses, J. Bonde, K. P. Jørgensen, J. H. Nielsen, S. Horch, I. Chorkendorff and J. K. Nørskov, *J. Am. Chem. Soc.*, 2005, **127**, 5308–5309.
51 J. D. Benck, T. R. Hellstern, J. Kibsgaard, P. Chakthranont and T. F. Jaramillo, *ACS Catal.*, 2014, **4**, 3957–3971.
52 Z. Gholamvand, D. McAteer, A. Harvey, C. Backes and J. N. Coleman, *Chem. Mater.*, 2016, **28**, 2641–2651.
53 G. R. Bhimanapati, T. Hankins, Y. Lei, R. A. Vilá, I. Fuller, M. Terrones and J. A. Robinson, *ACS Appl. Mater. Interfaces*, 2016, **8**, 22190–22195.

View Article Online
DOI: 10.1039/C9NR04974F

For Table of Contents Only